Spectroscopy and Photochemical Dynamics of the CF_3S Radical

David E. Powers, Michael B. Pushkarsky, Min-Chieh Yang, and Terry A. Miller*

Laser Spectroscopy Facility, Department of Chemistry, The Ohio State University, 120 W. 18th Avenue, Columbus, Ohio 43210

Received: July 8, 1997; In Final Form: October 16, 1997[⊗]

The CF_3S radical has been investigated using the LIF and fluorescence depletion techniques. The vibrational structure of the first excited $\tilde{A}\ ^2A_1$ state has been assigned. The photodissociation process at energies above the origin of the $\tilde{A}$ state has been characterized by fluorescence temporal decay and fluorescence depletion spectroscopy. Above the photodissociation threshold, the ratio of the rates for the competing processes of emission and dissociation varies strongly with both energy and vibrational mode.

I. Introduction

Methoxy, CH_3O,[1−10] and its F- and S-substituted derivatives, CH_3S,[11] CF_3O,[12−15] and CF_3S, form a remarkably fascinating family of free radicals from a number of perspectives. Several members are known, or speculated, to be key intermediates in chemical reactions relevant to combustion[16−19] and atmospheric pollution.[14,20−30] In recent years there has been a dramatic increase in spectroscopic and kinetic studies of the perfluoroalkoxy radicals motivated by the search for alternative compounds to the chlorofluorocarbons (CFC's) that deplete the atmospheric ozone. Since the perfluoroalkoxy radicals are thought to be intermediates in the atmospheric degradation of some alternatives to the CFCs, unambiguously analyzed spectra and information concerning their photochemical precesses are valuable for the monitoring of the radicals in reactions of environmental importance and for understanding their chemistry. In particular the precise determination of the threshold for their photochemical decomposition may be key information for the determination of the atmospheric fate of these radicals. From a theoretical perspective, the ground states of these radicals are all ^2E with C_{3v} symmetry and hence subject to the competitive effects of Jahn−Teller distortion and spin−orbit coupling.[2,3] Even for the simplest and best studied radical, CH_3O, these interactions are not yet completely understood.[4,6]

As the spectroscopy of these species has gradually progressed, their photochemistry has attracted ever increasing interest. The ground-state surfaces of the hydrides are known[31] to contain another minimum corresponding to the isomeric species, CH_2-XH, where X = O or S. The first excited $\tilde{A}\ ^2A_1$ state is expected to undergo photofragmentation with at least three channels identified[32] for methoxy: CH_3+ O, CH_2 +OH, and CH_2O+H, with all the products being in their ground electronic states. Analogous photofragmentation channels are expected for the remainder of the family. In a previous work,[33] we applied the fluorescence depletion spectroscopy (FDS) technique to the methoxy radical and observed its mode and frequency selective photofragmentation.

Recently we reported preliminary data on the spectroscopy and photochemistry of the CF_3S radical.[34] In this paper we report a more detailed picture of the spectroscopy of the $\tilde{A}\ ^2A \rightleftarrows \tilde{X}\ ^2E$ electronic transition and the mode and frequency selective photochemical decomposition of the heaviest member of the methoxy family, CF_3S, using both the laser-induced fluorescence (LIF) and FDS techniques. We assign the vibrational structure of this electronic transition and show that certain of these levels undergo selective predissociation or fragmentation. We use temporal profiles of the fluorescing vibrational states and the lifetime broadening in the FDS spectra of rapidly dissociating vibrational states to obtain information about the photochemistry of CF_3S.

II. Experimental Section

The CF_3S radicals were produced by ArF excimer laser (∼600mJ/cm^2 per pulse) photolysis of $(CF_3S)_2$ (PCR) entrained in a He expansion with a reservoir pressure of 7 atm and with the partial pressure of $(CF_3S)_2$ being provided by its vapor pressure at −60 °C. A General Valve with a nominal 0.7 mm diameter opening was pulsed for the expansion. In these experiments, two different configurations of the experimental apparatus were utilized. The first configuration has been described previously[2,11,15] and has been routinely used to record laser excitation and dispersed fluorescence spectra. The spectroscopic laser was a Lumonics Hyperdye dye (HD 300) laser pumped by a Lambda Physik (EMG103MSG) excimer laser. To record the excitation spectra, the dye laser was scanned, under computer control, and the resulting molecular fluorescence was collected perpendicular to the dye laser beam by a photomultiplier tube (EMI9659QB). The relative calibration of the features in this study was performed using a Burleigh wavemeter (model WA45000). Temporal measurements of the fluorescence decay were obtained in this configuration by time resolving the photomultiplier output with a LeCroy 2262 transient digitizer (80 MHz). For this experiment all imaging optics were removed to make sure that a negligible number of molecules exited the viewing region before radiating.

The FDS experiments required a more complex experimental arrangement previously described elsewhere[34] and illustrated in Figure 1. The basis of the FDS experiment rests on the following principles. The jet is crossed about 20 mm downstream from the nozzle with the "probe" laser (PL). The PL is fixed at the frequency of a transition originating from the vibrationless level of the $\tilde{X}$ state and terminating on a strongly fluorescing level of the $\tilde{A}$ state; e.g., for these experiments $\nu_3' = 3$. A second "depletion" laser (DL) was sent through the expansion, counterpropagating along the probe laser. The frequency of the DL is scanned as the total laser induced fluorescence from the $\tilde{A}$ state is monitored by a gated intensified CCD camera (Princeton Instruments model ICCD-1024MLDG-E). Since the DL, with a near-saturating pulse energy of 3−4 mJ/pulse focused to a 2 mm spot, is fired approximately 50 ns

[⊗] Abstract published in *Advance ACS Abstracts,* December 1, 1997.

S1089-5639(97)02202-0 CCC: $14.00

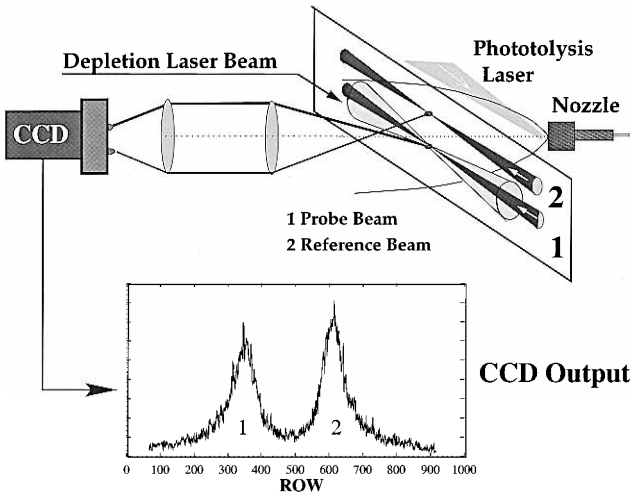

Figure 1. Schematic diagram showing the details of the arrangement of the probe and depletion beams and the free jet expansion. The spatially resolved image of the laser-induced fluorescence from the jet is imaged on the CCD, with output as indicated. The signal is subsequently processed as described in the text.

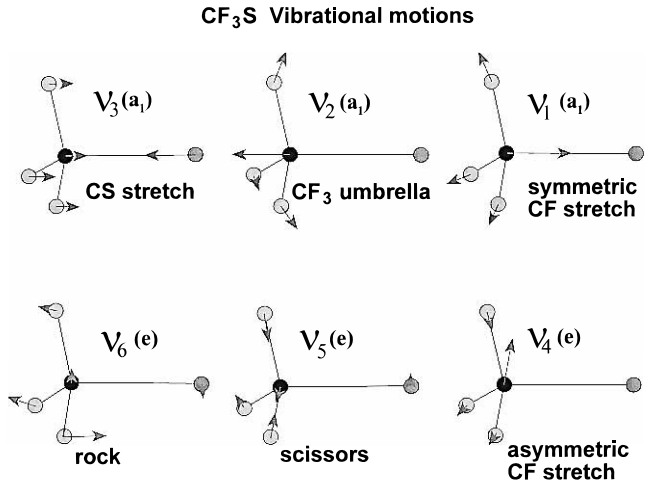

Figure 2. Schematic representation of the atomic motions in the a_1 and e symmetry vibrational modes in CF_3S.

before the PL, when it is on resonance with a transition originating from the vibrationless level of the ground state it will significantly deplete the population of that level prior to its being probed by the PL. If the upper level of the DL transition does not fluoresce appreciably (as is the case for photofragmenting levels), this DL-pumped transition will result in a decrease in ground-state population, and one will observe a negative-going signal (see below for the details of the signal monitored). Should the transition excited by the DL have a strongly fluorescing $\tilde{A}$ state terminal level, the DL and PL excited fluorescence will combine to produce a net increase in detected fluorescence with an observed positive-going signal. Upper state levels with competitive radiative and nonradiative pathways can appear as either positive- or negative-going signals, depending upon the relative rates of the two processes.

In any laser double-resonance experiment a key difficulty is to distinguish between changes in the intensity of the fluorescence from the PL caused respectively by the DL and random fluctuations from other sources, e.g., shot-to-shot variations in radical production, PL intensity, etc. To cancel the latter effects, we split the PL into two equal beams, each of 0.5 mJ/pulse energy, focused to ~1 mm diameter spots in spatially separate but equivalent regions of the expansion. The fluorescence from each of the two lasers is imaged on the two-dimensional array of pixels of the intensified CCD as shown in Figure 1. The CCD is allowed to accumulate signal for a period of time necessary to achieve a good signal-to-noise (typically 50 laser shots are needed). The signal-to-noise was improved by the ability to have the intensifier on only during the period of radical fluorescence. After the accumulation time the charge on the pixels is downloaded. The process of downloading the data from the CCD is performed row by row (not pixel by pixel) in the hardware supplied with the CCD camera. This has the advantage of allowing the total charge on a row of pixels to be accumulated quickly in hardware prior to the slower transfer process thereby minimizing the number of data points that need to be transferred to the computer. By performing this accumulation, the data is reduced to a one-dimensional array as shown in the insert of Figure 1. This array is then downloaded to a computer that will later integrate the intensity under each of the two peaks. The DL is overlapped with one of the matched spots of the PL and fired ~50 ns prior to the PL. With the PL fixed on resonance, in the absence of a resonance for the DL, the output is as shown in Figure 1.

We define the observed signal S to be given by

$$S = \frac{I_1}{I_2} \tag{1}$$

where I_1 and I_2 are the integrated areas of the peaks in the insert of Figure 1. When the scanned DL frequency is in resonance with a nonfluorescing excited state, the peak labeled 1, corresponding to the image from PL beam 1, is significantly reduced due to depletion of ground-state radicals by the DL, while the image labeled 2 remains unchanged; hence S drops below unity. On the other hand, a DL resonance with a fluorescing state causes S to increase above unity.

III. Vibrational Assignments of the $\tilde{A}\ ^2A_1$ State

The CF_3S radical, like the other members of the methoxy radical family, has six normal vibrational modes, three totally symmetric a_1 vibrations, and three doubly degenerate e symmetry vibrations. Figure 2 displays the atomic displacements for vibrational modes of CF_3S based upon ab initio calculations[35] for the $\tilde{A}$ state using a ROHF/6-31G* basis set. Although one can qualitatively describe these modes as the symmetric C−F stretch (ν_1), the CF_3 umbrella motion (ν_2), and the C−S stretch (ν_3), one can see by the atomic displacements shown in Figure 2 that all three of the a_1 symmetry modes involve a significant change in the C−S bond length. Since our previous rotational analysis[36] of the origin band of CF_3S shows a significant change in the length of the C−S bond between the $\tilde{A}$ and $\tilde{X}$ states, it is no surprise that the LIF spectrum shows strong progressions in each of these three modes. The three degenerate e modes can be described as the asymmetric C−F stretch (ν_4), the C−F scissors bend (ν_5), and the CF_3 rock (ν_6), although again significant mixing is indicated by the atomic displacements shown in Figure 2. Transitions from the vibrationless level of the $\tilde{X}\ ^2E$ ground state to the three e modes in the $\tilde{A}\ ^2A_1$ excited state are normally forbidden, but the Jahn−Teller interaction in the ground state mixes some e vibrational character into the vibrationless level and transitions to some e modes in the electronic state may become allowed. In fact, the transitions to the fundamentals of ν_5 and ν_6 are observed as well as combinations and overtones of these modes with the a_1 modes and each other.

The assignment of the excited electronic state vibrational frequencies from the LIF spectrum is not as straightforward as

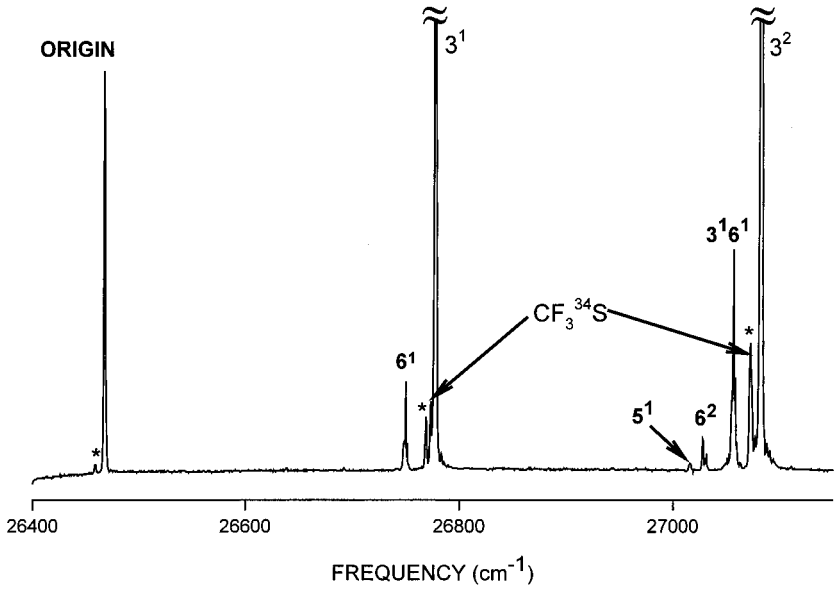

Figure 3. Portion of the LIF spectrum of the $\tilde{A}\ ^2A-\tilde{X}\ ^2E$ electronic transition of CF_3S. In addition to "cold" transitions in $CF_3{}^{32}S$, other features that are indicated include the $CF_3{}^{34}S$ isotopomer and He complexes with CF_3S (indicated by a star).

one might expect. Complications arise from several factors. The existence of observed transitions to the fundamentals of five of the six normal modes, combined with the presence of a large number of combinations and overtones with observable oscillator strength, results in a multitude of vibronic transitions to the $\tilde{A}$ state. In addition, all five of the observed modes have a fundamental frequency of less than about 1000 cm^{-1}. Ergo within the first few thousand cm^{-1} above the excited-state origin, the density of vibrational states is rather large and transitions to nearly all these levels are allowed, making assignments difficult for many of the transitions.

A further complication results from the presence of lines from various species. Besides the transitions from the most abundant ^{32}S isotopomer, the ^{34}S isotopomer, with a natural abundance of about 5%, yields observable lines for some of the stronger transitions. Additional observed lines arise from hot vibrational bands as well as from $CF_3S{\cdot}He$ complexes that are present. At low backing pressure, there are a large number of hot bands present in the spectrum. At higher backing pressures these hot bands decrease in intensity but $CF_3S{\cdot}He$ cluster features grow in. Most of these transitions can be sorted out by varying the expansion conditions and observing the relative changes in the spectra, but with so many observed transitions, it is often challenging, especially at higher energies.

Figure 3 shows a trace of the first 700 cm^{-1} of the LIF spectrum for CF_3S, illustrating some of the complications mentioned above. In this figure the fundamentals of three of the modes (ν_3, ν_5, and ν_6) and several combinations and overtones are visible. This spectrum was taken under conditions that minimize hot bands but enhance cluster formation, and several lines from clusters are visible in the spectrum. One can see in this spectrum that the fundamentals of ν_3 and ν_6 are sufficiently close in frequency, as is the frequency of ν_5 with two quanta of either of the former, so that a grouping of transitions occurs adding congestion to certain regions of the spectrum.

The positions of the experimentally observed, cold bands of CF_3S with their vibronic assignment (see below) are summarized in Table 1. Hot bands and inert gas containing complexes, where identifiable, have been omitted from the table. Table 1 includes the frequencies for bands observed by both the LIF and the FDS technique and are marked L and D respectively in the table. Since the rotational structure was not resolved in this experiment the frequencies of the bands were chosen to be the center of the band. The frequencies in Table 1 represent the energy relative to the vibrationless level of the $\tilde{A}\ ^2A_1$ state, which was determined from the rotationally resolved spectrum[36] to be 26 393.16 cm^{-1} above the common origin of the two spin−orbit components of the ground state. The actual position of the lowest frequency transition in the observed, rotationally resolved spectrum was 26 473.16 cm^{-1}, which is 80 cm^{-1} (half of the ground-state spin splitting) higher than the true origin of the ground state since all the observed transitions arise from the lower $^2E_{3/2}$ component.

A. Totally Symmetric Modes. As mentioned above, the rotational analysis[36] of CF_3S indicates that there is a significant lengthening of the C−S bond in the excited state relative to that in the ground state. The lengthening of this bond should give rise to progressions of vibrational modes that involve a change in the C−S bond which for CF_3S includes all three of the totally symmetric, a_1 modes (based on ab initio calculations[35]). Indeed overtones of all three of the a_1 symmetric modes are observed in the spectrum, precluding the assignment of a single strong progression to overtones of the C−S stretching mode. Assignments of the fundamentals of individual modes therefore rely heavily on a combination of ab initio calculations[37] and on the rotationally resolved spectra.[36] The unique rotational contours predicted for various bands, along with reasonable frequency predictions based upon the calculations, make the assignment of the members of these progressions fairly straightforward.

The lowest frequency totally symmetric band observed in the LIF spectrum is at 305 cm^{-1}. The justification for assigning this feature as an a_1 band can be found in the high-resolution rotationally resolved analysis of this band,[36] which establishes unambiguously that it must be a totally symmetric level. We assign this band as the fundamental of the nominal C−S stretch, ν_3, based largely upon the good agreement of this value with the ab initio calculation as shown in Table 2. Consistent with the C−S stretch assignment, a long progression of overtones for this band can be readily observed in the spectrum with members up to 3_0^4 seen in the LIF spectrum and an additional four-members observed using the FDS technique.

The CF_3 umbrella mode (ν_2) has been assigned to a strong LIF feature at 736 cm^{-1}. The high-resolution data again

TABLE 1: Vibrational Frequencies and Assignments[a] for the $\tilde{A}$ State of the CF_3S Radical

relative frequency[b]	technique[c]	assignment	relative frequency[b]	technique[c]	assignment
0	L	0^0	2062	D	$2^2 3^1 6^1$
282	L	6^1	2067	D	3^7
305	L	$3^1(^{34}S)$	2081	L	
310	L	3^1	2092	L,D	$2^2 3^2$
549	L	5^1	2137	L,D	$1^1 3^1 6^3$
561	L	6^2	2148	D	$1^1 3^2 5^1$
589	L	$3^1 6^1$	2159	D	$1^1 3^2 6^2$
604	L	$3^2(^{34}S)$	2167	D	$2^1 3^2 5^1 6^1$
615	L	3^2	2180	D	$1^1 3^3 6^1$
736	L	2^1	2194	D	$2^1 3^3 6^2$
824	L	$5^1 6^1$	2201	D	$1^1 3^4$
845	L	6^3	2210	L	2^3
856	L	$3^1 5^1$	2215	D	
866	L	$3^1 6^2$	2223	D	$2^1 3^4 6^1$
892	L	$3^2 6^1$	2240	D	$2^1 3^5$
897	L	$3^3(^{34}S)$	2253	L	$1^2 6^1$
914	L	3^3	2272	L	$1^1 2^1 5^1$
990	L	1^1	2282	L	$1^2 3^1$
1019	L	$2^1 6^1$	2301	L	$2^2 5^1 6^1$
1043	L	$2^1 3^1(^{34}S)$	2314	L,D	$1^1 2^1 3^1 6^1$
1048	L	$2^1 3^1$	2331	L	$2^2 3^1 6^2$
1130	L	$3^1 5^1 6^1$	2340	D	$1^1 2^1 3^2$
1148	L	$3^1 6^3$	2345	D	3^8
1160	L	$3^2 5^1$	2362	D	
1169	L	$3^2 6^2$	2371	D	$2^2 3^2 6^1$
1192	L	$3^3 6^1$	2393	D	$2^2 3^3$
1211	L,D	3^4	2455	L	$1^1 2^2$
1271	L	$1^1 6^1$	2457	D	$1^1 3^3 6^2$
1285	L	$2^1 5^1$	2477	L	$1^1 3^4 6^1$
1295	L	$2^1 6^2$	2492	D	$1^1 3^5$
1300	L	$1^1 3^1$	2514	D	$2^1 3^5 6^1$
1329	L	$2^1 3^1 6^1$	2525	D	$2^1 3^6$
1354	L	$2^1 3^2$	2559	L	$1^2 3^1 6^1$
1431	L	$3^2 5^1 6^1$	2586	L	
1447	L	$3^2 6^3$	2588	D	$1^2 3^2$
1457	D	$3^3 5^1$	2619	D	$1^1 2^1 3^2 6^1$
1466	D	$3^3 6^2$	2642	D	$1^1 2^1 3^3$
1474	L	2^2	2649	D	$2^2 3^2 6^2$
1485	D	$3^4 6^1$	2666	D	
1499	D	3^5	2675	D	$2^2 3^3 6^1$
1538	L	$1^1 5^1$	2689	D	$2^2 3^4$
1550	L	$1^1 6^2$	2701	L	$1^2 2^1$
1561	L	$2^1 5^1 6^1$	2718	D	
1580	L	$1^1 3^1 6^1$	2733	D	
1595	L	$2^1 3^1 5^1$	2740	D	
1599	L	$2^1 3^1 6^2$	2752	D	$1^1 3^4 6^2$
1606	L	$1^1 3^2$	2757	D	$1^1 2^2 3^1$
1634	L,D	$2^1 3^2 6^1$	2771	D	$1^1 3^5 6^1$
1654	D	$2^1 3^3$	2780	D	$1^1 3^6$
1724	L	$1^1 2^1$	2806	D	$2^1 3^7$
1741	D	$3^3 6^3$	2832	D	
1747	D	$3^4 5^1$	2867	D	$1^2 3^2 6^1$
1756	L	$2^2 6^1$	2885	D	
1786	L	$2^2 3^1$	2890	D	$1^2 3^3$
1786	D	3^6	2898	D	$3^7 5^1 6^1$
1813	L	$1^1 5^1 6^1$	2916	D	
1834	L	$1^1 6^3$	2922	D	$1^1 2^1 3^3 6^1$
1846	L	$1^1 3^1 5^1$	2934	D	
1856	L	$1^1 3^1 6^2$	2941	D	$1^1 2^1 3^4$
1866	L	$2^1 3^1 5^1 6^1$	2943	L	1^3
1872	L		2962	D	
1883	L,D	$1^1 3^2 6^1$	2980	D	$2^2 3^5$
1896	D	$2^1 3^2 5^1$	3011	L	$1^2 2^1 3^1$
1900	L	$2^1 3^2 6^2$	3016	D	
1905	L,D	$1^1 3^3$	3045	D	
1927	D	$2^1 3^3 6^1$	3051	D	$1^1 2^2 3^2$
1949	D	$2^1 3^4$	3062	D	$1^1 3^7$
1972	L	1^2	3078	D	
2005	L	$1^1 2^1 6^1$	3082	D	$2^1 3^8$
2035	L	$1^1 2^1 3^1$			

[a] A few features could not be readily assigned, and for these no value is indicated in the assignment column. We were unable to determine if these features were from hot or cold bands. [b] All frequencies in cm^{-1}. The estimated error in the measurement of the relative frequency is 1 cm^{-1}. [c] Labels indicate the technique by which transitions to the levels were detected, L for LIF and D for FDS.

TABLE 2: Frequencies (cm^{-1}) of the Vibrational Modes of the $\tilde{A}$ State of the CF_3S Radical

mode	G(1)	ω_e[a]	$\omega_e x_e$[b]	ω_e (calcd)[d]
ν_1	989.0	998(2)	3.64(4)	1025
ν_2	736.0	740(2)	0.50(4)	747
ν_3	308.5	314.0(5)	2.40(4)	340
ν_4				1352
ν_5	548.0	*c*		561
ν_6	282.0	277(2)	−0.9(5)	306

[a] The errors correspond to 1 standard deviation obtained from the least-squares fit (See section III.D). [b] The following nondiagonal anharmonic parameters (cm^{-1}) were obtained from the fit: $\omega_e x_{e12} = 3.4(7)$, $\omega_e x_{e13} = -0.7(2)$, $\omega_e x_{e23} = -0.4(2)$. [c] Insufficient number of transitions were observed for this mode to determine ω_e and $\omega_e x_e$. [d] Calculated value.[37]

indicates that this is a transition to a totally symmetric vibration, and it is in very good agreement with the ab initio value as shown in Table 2. The fundamental of the third totally symmetric mode (ν_1) band has been assigned to the strong feature at 990 cm^{-1}. High-resolution data was again used to verify that this is a transition to an a_1 mode, and the frequency is in good agreement with the calculated value.

B. Non-totally Symmetric Modes. Transitions to the $\tilde{A}$ state non-totally symmetric, e modes from the vibrationless level of the ground state are normally symmetry forbidden in the $\tilde{A}\ ^2A_1-\tilde{X}\ ^2E$ electronic transition but, as mentioned earlier, can be allowed due to the Jahn−Teller distortion of the ground state. In CH_3O, for example, all three of the degenerate modes (for ν_4 only combinations are observed) are seen.[10] In CF_3S we see activity in two of the three e modes.

The fundamental of the lowest frequency e mode (ν_6) has been assigned to the band at 282 cm^{-1}. Even at the moderate resolution of this experiment, it is apparent that this mode has a considerably different rotational profile than that observed for the totally symmetric bands. The rotationally resolved high-resolution data[36] verifies that this is in fact a transition from a vibronic e level of the $\tilde{X}$ state to a vibronic *e* level of the excited $\tilde{A}$ state. Ab initio calculations place the ν_6 fundamental band at 306 cm^{-1} (Table 2), in good agreement with the measured value.

The second lowest frequency e mode (ν_5) has been assigned to a weak feature at 549 cm^{-1}. The symmetry of this vibration has been verified by the rotationally resolved spectrum,[36] and the frequency is in good agreement with the ab initio calculations (see Table 2).

C. Combinations and Overtones. Many combinations and overtones have been observed and assigned in the LIF and FDS spectra. Overtones of ν_3 are observed by LIF and FDS up to 3_0^8. The overtones of ν_2 and ν_3 are both observed to three quanta. Also observed are the first three members of the progression of the e vibrational mode ν_6. In addition to the overtones, there are many combination bands, the most extensive of which involve a progression in ν_3 combined with one quantum of the other modes. The combination of the LIF and FDS techniques make it possible to map the transitions to the fluorescing bright states as well as to the dark photofragmenting ones. Usually most of these long progressions have the first couple of members observed in LIF, while FDS is required to observe the higher frequency members. The combined data from LIF and FDS shows that for these long progressions the nonradiative decay of the higher members does not contribute to any noticeable perturbations in their frequencies. In other words the same set of vibrational parameters can be used to describe the positions of both bright and dark members of progressions. Frequencies and assignments for all the observed transitions are summarized in Table 1.

D. Anharmonic Oscillator Model. The combined LIF and FDS spectra reveal a rich vibrational structure involving five normal modes and their combinations. The three totally symmetric modes were observed in combinations with each other and in overtones up to three quanta of ν_2 and ν_1 and eight quanta of ν_3. The standard anharmonic model Hamiltonian (complete through second-order perturbation theory in the absence of Fermi resonances) was used to fit the experimental data for the three symmetric modes.

$$E(\nu_1, \nu_2, \nu_3) = T_0 + \omega_{e1}(\nu_1 + {}^1/_2) + \omega_{e2}(\nu_2 + {}^1/_2) + \omega_{e3}(\nu_3 + {}^1/_2) - \omega_e x_{e11}(\nu_1 + {}^1/_2)^2 - \omega_e x_{e22}(\nu_2 + {}^1/_2)^2 - \omega_e x_{e33}(\nu_3 + {}^1/_2)^2 - \omega_e x_{e12}(\nu_1 + {}^1/_2)(\nu_2 + {}^1/_2) - \omega_e x_{e13}(\nu_1 + {}^1/_2)(\nu_3 + {}^1/_2) - \omega_e x_{e23}(\nu_2 + {}^1/_2)(\nu_3 + {}^1/_2) \quad (2)$$

where the above symbols have their standard significance. This model was sufficient to fit, within 2 experimental standard deviations, the positions of all observed bands, corresponding to the excitations of no more than two different modes. This analysis involved the 10 parameters of eq 2 to fit about 40 experimental points. The model failed to predict as accurately the positions of a few bands assigned as combinations involving all three totally symmetric modes. Those bands were excluded from the final fit, as their fitting would have required the introduction of a large number of additional interaction parameters, for which there was insufficient experimental data for a determination. As it has been mentioned above, both bright and dark states were used in fitting. There was no evidence that positions of the levels corresponding to dark states exhibit any deviations beyond the experimental error from the anharmonic model fit. The best least-squares fit parameters including the three harmonic frequencies ω_e and six anharmonic constants $\omega_e x_e$ are summarized in the Table 2 as well as values of $G(1)$ (the energy of the first excited level of a given mode above the origin) for all five observed modes. In addition, values are given in Table 2 for ω_{e6} and $\omega_e x_{e6}$ from a separate fit to the conventional single-mode-anharmonic model, as well as a value of G(1) for ν_5.

IV. Photofragmentation

A. Data Analysis. With the assignments of the vibronic bands relatively completely accomplished, we can now turn to the fate of the radicals placed in the various vibronic levels of the $\tilde{A}$ state. The decay of the vibrational levels with low energy content ($\lesssim$1200 cm^{-1}) appears unique. They simply emit a photon with a radiative lifetime of just less than 3 μs. However for levels of higher energy content ($\gtrsim$1200 cm^{-1}), it appears that there is also a nonradiative decay path available with widely differing radiative/nonradiative branching ratios depending upon the particular level excited. We presume that this nonradiative decay is accomplished via photofragmentation of the radical. Theory[37] indicates that this fragmentation occurs along the C−S bond.

To provide a quantitative measure of the probabilities for radiative decay and photofragmentation we turn to measurements of the individual levels' lifetimes. For the levels observed by LIF the lifetime measurement is via straightforward monitoring of the temporal evolution of the fluorescence, with a subsequent fitting of the exponential decay to yield the natural lifetime, τ_v, of the vibrational level. The fraction of molecules that radiate (quantum yield) is found by the ratio of τ_v/τ_0 where τ_0 is the radiative lifetime of the $\tilde{A}$ state. We approximate τ_0 as the measured lifetime, 2.74 μs, of the vibrationless level. This approximation seems valid as the τ_v's of all measured levels below 1000 cm^{-1} are quite similar to this value. The values of all the τ_v's measured by LIF are given in Table 3, and the log of the ratios are plotted in Figures 4 and 5. (Lifetime measurements were not made on all the observed levels in the LIF spectrum since the signal was too weak to obtain good values for many of the features when the fluorescence pickup optics were removed as described in section II.) The error in the lifetime values is estimated as 5% of the value of the lifetime.

For those levels observed solely in FDS, measuring the lifetime of the state is somewhat more complicated. In principle, for those lines for which lifetime broadening is observed, a lifetime determination is possible; for those absent such broadening, it is not. A couple of important points, however, must be made about the observed widths. With the resolution of the current experiment individual rotational lines are not

TABLE 3: Measured Lifetimes for the $\tilde{A}$ State of the CF_3S Radical

assignment	lifetime[a]	assignment	lifetime[a]
0^0	2.74 (14) μs	3^7	2.3 (5) ps
3^1	2.88 (14) μs	$2^2 3^2$	100 (5) ns
3^2	2.95 (15) μs	2^3	429 (21) ns
2^1	2.62 (13) μs	$2^1 3^5$	4.5 (16) ps
3^3	2.54 (12) μs	$1^2 3^1$	928 (46) ns
1^1	2.67 (13) μs	3^8	1.1 (2) ps
$2^1 3^1$	2.67 (13) μs	$1^1 2^2$	130 (6) ns
3^4	38 (15) ns	$1^1 3^5$	5.5 (32) ps
$1^1 3^1$	2.71 (14) μs	$2^1 3^6$	2.9 (5) ps
$2^1 3^2$	333 (16) ns	$1^1 3^6$	2.2 (3) ps
2^2	2.18 (11) μs	$2^1 3^7$	1.9 (4) ps
$1^1 3^1 6^1$	2.68 (13) μs	$1^1 2^1 3^4$	2.7 (5) ps
$1^1 3^2$	821 (41) ns	1^3	1.30 (6) μs
$1^1 2^1$	2.53 (13) μs	$1^1 3^7$	2.6 (5) ps
1^2	2.49 (12) μs	$2^1 3^8$	0.9 (2) ps
$1^1 2^1 3^1$	607 (15) ns		

[a] Those lifetime with values greater than 1 ns were measured by fluorescence temporal decay. All other lifetimes were determined by broadening in the FDS spectra.

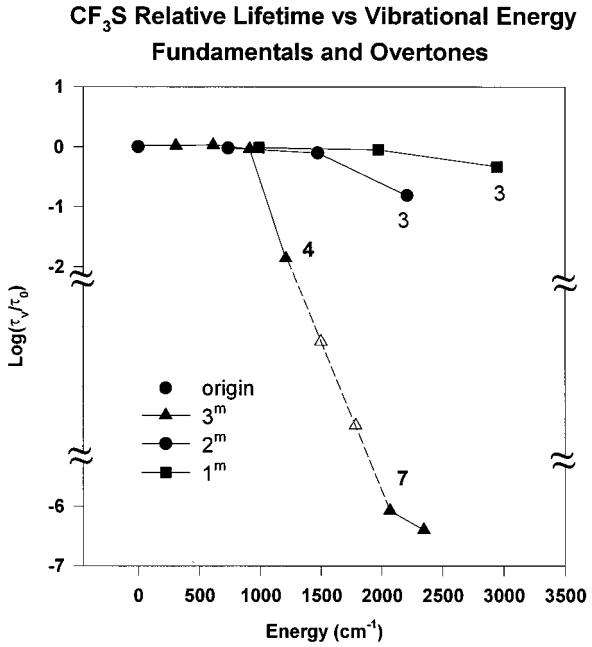

Figure 4. Log of the fluorescence quantum yield (τ_v/τ_0) for fundamentals and overtones of the symmetric modes plotted vs their energy above the vibrationless level of the $\tilde{A}$ state. The sharp contrast between the behavior of ν_3 and the rest of the symmetric modes is easily observed. The lifetimes of 3^5 and 3^6 were not determinable, so we have placed the vertical position of these points on the line connecting 3^4 and 3^7 for convenience, with the horizontal position located at the level's energy.

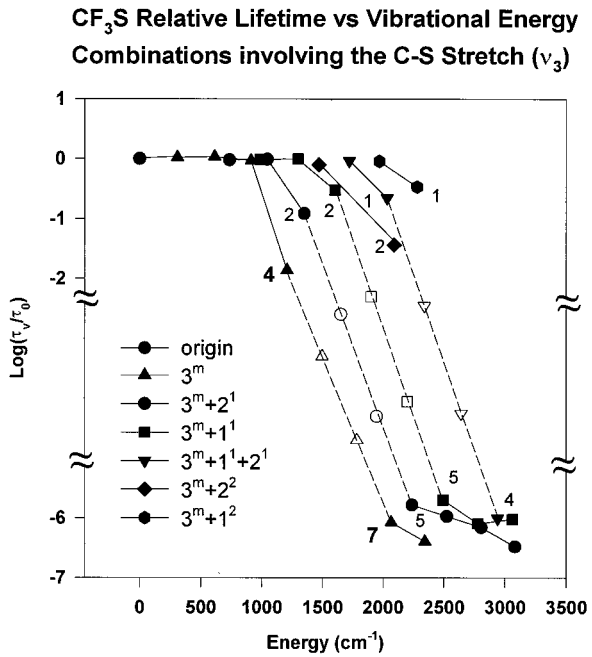

Figure 5. Fluorescence quantum yield for numerous combination bands vs relative energy above the origin of the $\tilde{A}$ state. The number of quanta in ν_3 is indicated for the level with the lowest quantum yield that is observed by LIF. The vertical positioning of the nonfilled symbols is accomplished in the manner described in the caption of Figure 4.

resolved. Instead we observe a rotational contour for each band. The rotational contours for all of the bands of a_1 symmetry vibronic levels are fairly uniform. The transitions to e symmetry vibronic levels are not nearly so regular and uniform, but in general are much broader than the corresponding a_1 ones and even at the resolution of this experiment show some partially resolved rotational structure. As a result the widths for the transitions to e symmetry modes could not be fit to any generic line shape function without a large error in the parameter values, and in addition within the error there is, with only a few exceptions, no observable lifetime broadening in these features. Thus in our analysis only the bands involving symmetric levels were used in the lifetime determinations from line broadening in the FDS experiments.

In fitting the contour of the lifetime broadened a_1 bands, it is important to recognize that the experimentally measured contour is a convolution of the unresolved rotational contour and the homogeneous broadening of each rotational line due to nonradiative decay. The LIF-observed features, whose temporal decay can be measured and for which it is known that the lifetime broadening is negligible within our resolution, are well fit by a Gaussian distribution with parameters A_g, ω_0, and σ_g

$$f_g(\omega) = A_g\, e^{-(\omega-\omega_0)^2/2\sigma_g^2} \tag{3}$$

where ω_0 is the band center, A_g its normalization constant, and $2\sigma_g(\ln 4)^{1/2}$ is the fwhm of the band.

The lifetime broadening of individual rotational lines gives rise to a Lorentzian line shape

$$f_L(\omega) = \frac{A_L}{1+\left(\dfrac{\omega-\omega_0}{\sigma_L}\right)^2} \tag{4}$$

where $2\sigma_L$ is equal to the fwhm of the line and is related to the lifetime, τ, by the formula[38,39]

$$\tau = (4\pi c\sigma_L)^{-1} \tag{5}$$

where σ_L is expressed in cm^{-1} and c is the speed of light.

If one makes an assumption that all rotational lines in the vibronic band decay with the same rate, the resultant line shape of the vibrational feature is the convolution of the homogeneous (Lorentzian) line profile and the inhomogeneous (Gaussian) distribution, which results in the well-known Voigt contour[40] that is explicitly expressed in terms of Gaussian σ_g and Lorentzian σ_L widths as follows

$$f_V(\omega) = A_V \int_{-\infty}^{\infty} \frac{e^{-y^2}}{\left(\dfrac{\sigma_L}{\sqrt{2}\sigma_g}\right)^2 + \left(\dfrac{\omega-\omega_0}{\sqrt{2}\sigma_g} - y\right)^2}\, dy \tag{6}$$

where y is a dimensionless dummy integration variable and A_V is the normalization constant.

The first step of the analysis is to determine a value of the Gaussian line width parameter σ_g for a lifetime-unbroadened distribution of rotational lines. Fortunately in the observed spectra there is a band (3_0^4) observed in both the LIF and FDS spectra. By fitting 7 independent traces of 3_0^4 and 3_0^5 (which has the same width) to the Gaussian contour, eq 3, an average value of $\sigma_g = 0.61(13)$ cm^{-1} was determined and used as the width of an "unbroadened" FDS feature. Additional transitions to symmetric levels of the $\tilde{A}$ state seen in both LIF and in FDS, e.g., $1_0^1 3_0^3$ and $2_0^2 3_0^2$, as well as a number of bands seen only in LIF, were fit as Gaussians and found to be in good agreement with this line width parameter. As the final step of the analysis the contour of every feature seen in depletion was fitted to the Voigt function, eq 6, with the fixed value of $\sigma_g = 0.61$ cm^{-1} with the remaining parameters σ_L, ω_0, and A_V varied.

For the case when the band of interest was overlapped by other bands, the overall spectrum was simulated and fit with as many Voigt functions as observed lines. However, for practical purposes, nearly all studied bands were simulated and fit as either a simple peak or as a superposition of two only partially overlapping peaks. The lifetimes, reported in Table 3, were then calculated from the homogeneous line width parameter σ_L using eq 5. All fits were performed using the Peakfit program[41] which enables simultanous fitting of multiple features using Gaussian, Lorentzian, or Voigt funtions.

All the experimental traces of a given band were fit separately yielding unique values of σ_L for every experimental trace. The number of values of σ_L so obtained varied from two to seven depending upon the transition. The error in the reported values for σ_L was estimated according to the following procedures. Two sources were considered: the variation in σ_L from trace to trace and the propagation of the error in σ_g. The former would be easily estimated from the standard deviation of the individual measurements of σ_L. To estimate the latter error, each experimental trace was refit with $\sigma_g = 0.48$ and 0.74 cm^{-1}, respectively, 1 standard deviation below and above the best fit value of σ_g. The standard deviation of these fits was combined with the standard deviation of the trials via the standard formula of the square root of the sum of the squares. This approach likely gives a modest overestimate of the true error, since the variation in the observed σ_L values is not completely independent of the determined value of σ_g.

B. Discussion. We begin our discussion of the observed photofragmentation trends with a description of the most prominent ν_3^n progression. Although the overtones of ν_3 are only observed up to 3_0^4 using LIF, the FDS spectrum demon-

strates that the Frank Condon overlap and hence the oscillator strength of transitions up to 3_0^8 is considerable. This long progression is consistent with the significant lengthening of the C−S bond, by over 0.121 Å upon excitation to the $\tilde{A}$ state, as determined from the rotationally resolved spectrum.[36] The loss of intensity in the LIF spectrum beginning at 3_0^4 is therefore attributed to a coupling to the dissociative continuum similar to that reported for the methoxy radical.[33]

As can be seen from Table 3, by increasing the excitation in ν_3 from one to eight quanta, the lifetime is reduced by 6 orders of magnitude. In Figures 4 and 5 these data, as well as that for other progressions, is displayed by plotting the log of the quantum yield, i.e., log of the relative lifetimes, τ_v/τ_0, vs the vibrational energy (above the $\tilde{A}$ state vibrationless level), where τ_0 is the lifetime of the vibrationless level of the $\tilde{A}$ state. These figures show clearly the behavior of the quantum yield vs excitation energy for different vibrations.

Figure 4 shows the behavior of the quantum yield for the totally symmetric fundamentals and their overtones. It clearly illustrates how important is the distribution of the vibrational energy as well as its total value. For the ν_3 mode we see a distinct threshold behavior; $3\nu_3$ at 914 cm^{-1} shows no indication of a nonradiative photofragmentation process, while for $4\nu_3$ at 1211 cm^{-1}, it appears that $\gtrsim$98% of the radicals decay by dissociation rather than photon emission. As one continues to increase the number of quanta in ν_3, the photofragmentation process becomes ever more dominant, with less than one in a million molecules escaping fragmentation with $\gtrsim$2000 cm^{-1} of energy present in ν_3.

The behavior of the other two symmetric modes, ν_1 and ν_2, is in sharp contrast to that of ν_3. One can note from Figure 4 that putting nearly 3000 cm^{-1} of energy into ν_1 barely reduces the quantum yield (to approximately 50%), while considerably less energy into ν_3 effectively eliminates ($<10^{-6}$) emission. Much the same story is evident for ν_2. At energies greater than those where ν_3 has a $\lesssim$1% quantum yield, the second overtone of ν_2 decays almost exclusively by fluoresence, and even the third overtone has significant radiative decay.

As shown in Figure 2, ν_3 is predominately the C−S stretch. Since it is expected that the nonradiative decay involves breaking the C−S bond, it is reasonable to expect that ν_3 would be most effective in promoting this decay mechanism. However, what is rather surprising is how ineffective even excess energy is, when stored in the other symmetric modes. It appears that an energy criteria alone is insufficient to explain the onset of photofragementation. Rather it appears that dual criteria must be satisfied, sufficient energy and sufficient geometric extension along the reaction coordinate, which appears to coincide closely with the C−S bond stretch. In future work we will explore whether it is possible to quantify this relationship.

Figure 5 further illuminates our picture of the mode selectivity of the bond-breaking process in the $\tilde{A}$ state of CF_3S. It shows the differing behaviors of the various combination levels. While it again demonstrates that increasing total energy enhances fragmentation, how that energy is distributed among vibrational motions appears an even more significant determinant for bond breaking. Several combination levels with total vibrational energy content above 2000 cm^{-1} show little or no evidence for fragmentation. Only when the additional requirement of two, or more generally three, quanta of ν_3 excitation is fulfilled does C−S bond rupture become the dominant decay mechanism. Even in these combination levels extreme mode selectivity is the rule, with levels at approximately the same energy exhibiting up to 10^6 variation in propensity for dissociation.

V. Conclusions

The vibrational structure of the $\tilde{A}\ ^2A-\tilde{X}\ ^2E$ electronic transition of the CF_3S radical is for the first time reported and analyzed in detail. Because transitions are observed to the fundamentals of five (of the possible six) modes, which are of low frequency ($<$1000 cm^{-1}), as well as their combinations and overtones, the spectrum of CF_3S is very rich. However a detailed vibrational analysis, relying in part upon the rotational contour fingerprints, has led to reliable assignments for the vast majority of all the observed bands. These assignments in turn yield values for the vibrational frequencies, anharmonicies, etc. of the observed modes.

This relatively complete understanding of the spectroscopy of CF_3S allows us to use the various vibrational levels, whose wave functions sample different portions of the $\tilde{A}$ state potential energy surface, to investigate in considerable detail the photochemistry of CF_3S. We have observed very strong mode selectivity in these dynamics. While total vibrational energy content is not unimportant, the most striking feature of our observations is the specific need to place energy directly into the ν_3 mode, which closely corresponds to the reaction coordinate for C−S bond breaking. At roughly constant total energy content, selectivity factors of up to nearly 10^7 are observed, depending upon the specific amount of excitation in ν_3. This result is consistent with very little communication between the normal modes, even at energies considerably greater than 1000 cm^{-1} above the threshold for dissociation.

It is also consistent with the dissociation process being dominated by a process producing $CF_3 + S$ as products, although the present experiment cannot confirm the nature of the products. Similarly since the present experiment was not performed in a rotationally resolved manner, no evidence is available with respect to *J* or *K* dependence of the dissociation. However, we do note that in our analogous but rotationally resolved experiment[33] on CH_3O no *J* or *K* dependence was seen for the (limited range of) experimentally observed levels.

The present results are consistent with but, in some ways, even more striking than the ones we recently reported for the CH_3O radical. We therefore speculate that striking mode selectivity may be the rule rather than the exception for many moderate-sized radicals (and other species) for energies only moderately above threshold as long as the rate for dissociation is not excessively high compared to radiative decay. (This latter condition should largely be satisfied for any system in which bond breaking occurs because of diabatic curve crossing—leading to "smallish" avoided crossings—and which therefore would, in the one-dimension diatomic limit, be described as predissociative.) In the future, we plan to investigate other systems of this nature to try to develop a better overall understanding of photochemical selectivity in the process of bond breaking.

Acknowledgment. The authors gratefully acknowledge the support of the National Science Foundation via Grant No. 9320909.

References and Notes

(1) Endo, Y.; Saito, S.; Hirota, E. *J. Chem. Phys.* **1984**, *81*, 122.

(2) Foster, S. C.; Misra, P.; Lin, T. Y. D.; Damo, C. P.; Carter, C. C.; Miller, T. A. *J. Phys. Chem.* **1988**, *92*, 5914.

(3) Liu, X.; Damo, C. P.; Lin, T. Y. D.; Foster, S. C.; Misra, P.; Yu, L.; Miller, T. A. *J. Phys. Chem.* **1989**, *93*, 2266.

(4) Chiang, S. Y.; Hsu, Y. C.; Lee, Y. P. *J. Chem. Phys.* **1989**, *90*, 81.

(5) Geers, A.; Kappert, J.; Temps, F.; Wiebrecht, J. W. *J. Chem. Phys.* **1990**, *93*, 1472.

(6) Geers, A.; Kappert, J.; Temps.; Sears, T. J. *J. Chem. Phys.* **1993**, *98*, 4297.

(7) Geers, A.; Kappert, J. Temps, F.; Wiebrecht, J. W. *J. Chem. Phys.* **1994**, *101*, 3618.
(8) Geers, A.; Kappert, J.; Wiebrecht, J. W. *J. Chem. Phys.* **1994**, *101*, 3634.
(9) Misra, P.; Zhu, X.; Hsueh, C.-Y.; Halpern, J. B. *Chem. Phys.* **1993**, *178*, 377.
(10) Powers, D. E.; Pushkarsky, M.; Miller, T. A. *J. Chem. Phys.* **1997**, *106*, 6863.
(11) Hsu, Y. C.; Liu, X.; Miller, T. A. *J. Chem. Phys.* **1989**, *90*, 6852.
(12) Francisco, J. S.; Williams, I. H. *Chem. Phys. Lett.* **1984**, *110*, 240.
(13) Li, Z.; Francisco, J. S. *Chem. Phys. Lett.* **1991**, *186*, 336.
(14) Clemitshaw, K. C.; Sodeau, J. R. *J. Phys. Chem.* **1989**, *93*, 3552.
(15) Tan, X. Q.; Yang, M. C.; Carter, C. C.; Williamson, J. M.; Miller, T. A.; Mlsna, T. E.; Anderson, J. D. O.; Desmarteau, D. D. *J. Phys. Chem.* **1994**, *98*, 2732.
(16) Warnatz, J. *Combustion Chemistry;* Springer-Verlag: New York, 1984.
(17) Grotheer, H. H.; Kelm, S.; Driver, H. S. T.; Hutcheon, R. J.; Lockett, R. D.; Robertson, G. N. *Ber. Bunsen-Ges. Phys. Chem.* **1992**, *96*, 1360.
(18) Driver, H. S. T.; Hutcheon, R. J.; Lockett, R. D.; Robertson, G. N.; Grotheer, H. H.; S., K. *Ber. Bunsen-Ges. Phys. Chem.* **1992**, *96*, 1376.
(19) Hagele, J.; Lorenz, K.; Rhasa, D.; Zellner, R. *Ber. Bunsen-Ges. Phys. Chem.* **1983**, *87*, 1023.
(20) Mellouki, A.; Jourdain, J. L.; Le Bras, G. *Chem. Phys. Lett.* **1988**, *148*, 231 and references therein.
(21) Atkinson, R.; Baulch, D. L.; Cox, R. A.; Hampson, R. F., J.; Kerr, J. A.; Troe, J. *J. Phys. Chem. Ref. Data* **1989**, *18*, 881.
(22) Nesbitt, F. L.; Payne, W. A.; Stief, L. J. *J. Phys. Chem.* **1988**, *92*, 4030.
(23) Atkinson, R.; Cox, R.; Lesclaux, R.; Niki, H.; Zellner, R. AFEAS Report 20; World Meteorological Organization Global Ozone Research Monitoring Project, 1991.
(24) Chen, J.; Zhu, T.; Niki, H. *J. Phys. Chem.* **1992**, *96*, 6115.
(25) Sehested, J.; Nielsen, O. J. *Chem. Phys. Lett.* **1993**, *206*, 369.
(26) Kelly, C.; Treacy, J.; Sidebottom, J. W.; Nielsen, O. J. *Chem. Phys. Lett.* **1993**, *207*, 498.
(27) Nielsen, O. J.; Sehested, J. *Chem. Phys. Lett.* **1993**, *213*, 433.
(28) Wallington, T. J.; Hurley, M. D.; Schneider, W. F. *Chem. Phys. Lett.* **1993**, *213*, 442.
(29) Maricq, M. M.; Szente, J. J. *Chem. Phys. Lett.* **1993**, *213*, 449.
(30) Sehested, J.; Nielsen, O. J.; Wallington, T. J. *Chem. Phys. Lett.* **1993**, *213*, 457.
(31) Curtiss, L. A.; L. D, K.; Pople, J. A. *J. Chem. Phys.* **1991**, *95*, 4040.
(32) Osborn, D. L.; Leahy, D. J.; Ross, E. M.; Neumark, D. M. *Chem. Phys. Lett.* **1995**, *235*, 484.
(33) Powers, D. E.; Pushkarsky, M. B.; Miller, T. A. *J. Chem. Phys.* **1997**, *106*, 6878.
(34) Powers, D. E.; Pushkarsky, M.; Miller, T. A. *Chem. Phys. Lett.* **1995**, *247*, 548.
(35) Barckholtz, T.; Miller, T. A. To be published.
(36) Yang, M.-C.; Williamson, J. M.; Miller, T. A. *J. Mol. Spectrosc.* **1997**.
(37) Cui, Q.; Morokuma, K. *Chem. Phys. Lett.* **1996**, *263*, 54.
(38) Demtroder, W. *Laser Spectroscopy, Basic Concepts and Instrumentation;* Springer-Verlag: Berlin, Heidelberg, New York, 1982.
(39) Pearson, J.; Orr-Ewing, A. J.; Ashfold, M. N. R.; Dixon, R. N. *J. Chem. Phys.* **1997**, *106* (14), 5850.
(40) Bernath, P. F. *Spectra of Atoms and Molecules;* Oxford University Press: Oxford, 1995.
(41) Jandel scientific software v3.11. SPSS, Inc., Chicago, IL, 60611.